IEICE TRANS. ELECTRON., VOL.E107–C, NO.10 OCTOBER 2024

PAPER *Special Section on Microwave and Millimeter-Wave Technologies*

Uniform Microwave Heating via Electromagnetic Coupling Using Zeroth-Order Resonators

Baku TAKAHARA[†], *Student Member*, **Tomohiko MITANI**[†a)], *Member*, *and* **Naoki SHINOHARA**[†], *Senior Member*

SUMMARY We propose microwave heating via electromagnetic coupling using zeroth-order resonators (ZORs) to extend the uniform heating area. ZORs can generate resonant modes with a wavenumber of 0, which corresponds to an infinite guide wavelength. Under this condition, uniform heating is expected because the resulting standing waves would not have nodes or antinodes. In the design proposed in this paper, two ZORs fabricated on dielectric substrates are arranged to face each other for electromagnetic coupling, and a sample placed between the resonators is heated. A single ZOR was investigated using a 3D electromagnetic simulator, and the resonant frequency and electric field distribution of the simulated ZOR were confirmed to be in good agreement with those of the fabricated ZOR. Simulations of two ZORs facing each other were then conducted to evaluate the performance of the proposed system as a heating apparatus. It was found that a resonator spacing of 25 mm was suitable for uniform heating. Heating simulations of SiC and Al_2O_3 sheets were performed with the obtained structure. The heating uniformity was evaluated by the width $L_{50\%}$ over which the power loss distribution exceeds half the maximum value. This evaluation index was equal to $0.397\lambda_0$ for SiC and $0.409\lambda_0$ for Al_2O_3, both of which exceed $\lambda_0/4$, the distance between a neighboring node and antinode of a standing wave, where λ_0 is the free-space wavelength. Therefore, the proposed heating apparatus is effective for uniform microwave heating. Because of the different electrical parameters of the heated materials, SiC can be easily heated, whereas Al_2O_3 heats little. Finally, heating experiments were performed on each of these materials. Good uniformity in temperature was obtained for both SiC and Al_2O_3 sheets.

key words: *metamaterial, microwave heating, electromagnetic coupling, wireless power transfer*

1. Introduction

Microwave heating is widely used for processing food [1], chemicals [2], wood [3], rubber [4], and ceramics [5], [6]. This method of heating is faster and more efficient than conventional heating methods because microwaves do not require a medium for heat transfer [7]. In the field of ceramics, research on sintering is of particular interest [8]. Nonuniform heating and thermal runaway are the main issues in the sintering of ceramics, because thermal runaway leads to high stress and material fracture [5], [9].

Microwave heating apparatuses can be classified into two categories: multimode and single-mode applicators. Multimode applicators, typified by microwave ovens, consist of a metal cavity with dimensions larger than the wavelength. Many modes are generated inside the cavity by the multiple reflections of the microwaves. However, some parts have a high electric or magnetic field intensity, depending on the shape of the applicator, the shape and electric constants of the heated object, and the location of the object in the applicator. Thus, nonuniform heating can occur easily, especially when the heated object is large [10].

To improve heating uniformity, studies have been conducted using stirrers [11], [12], turntables or conveyors [13], [14], and multiple input ports [15], [16]. In addition, the internal electromagnetic field can vary greatly even with only slight differences in the location of the heated object. It is difficult to precisely calculate the internal electromagnetic field distribution, and multimode applicators are not suitable for microwave heating processes that require strict temperature control [17]. Single-mode applicators generate standing waves inside the heating apparatus, making it possible to select between electric and magnetic fields for heating. In addition, the energy irradiated to the heated object can be calculated from the internal electromagnetic field distribution to enable strict temperature control. However, nonuniform heating is caused by the nodes and antinodes of the standing waves. When heating by an electric field, the heating power exceeds 50% of the peak value only in a region of width $\lambda_g/4$ centered on the peak position, where λ_g is the guide wavelength. This is because dielectric heating proceeds in proportion to the square of the electric field strength. The region is the same when heating by a magnetic field. Therefore, the size of the heated sample should be small for uniform heating.

In a previous study [18], the position of the standing wave was changed by moving the short-circuit plate attached to a waveguide in the range of $\lambda_g/4$ to make the time-averaged irradiation energy uniform. In another study [19], a square waveguide was partially filled with a dielectric to create a uniform electric field distribution by generating transverse electromagnetic (TEM) modes [20], and the resulting apparatus was applied to microwave heating. The challenges this approach poses, however, are the need for an object with an optimal dielectric constant and the large losses in the dielectric. In addition, no heating experiments were conducted in this study. In another study [21], a metal plate was inserted into a square waveguide to narrow the waveguide width and elongate the guide wavelength. However, if the waveguide width was too narrow, the resonant frequency was reduced to below the cutoff frequency, limiting the uniform heating area. Because of these characteristics, there is a need for heating apparatuses that can heat objects over a wide area with a single-

Manuscript received October 23, 2023.
Manuscript revised February 7, 2024.
Manuscript publicized April 9, 2024.

[†]Research Institute for Sustainable Humanosphere, Kyoto University, Uji-shi, 611–0011 Japan.
a) E-mail: mitani.tomohiko.3u@kyoto-u.ac.jp

DOI: 10.1587/transele.2024MMP0005

mode applicator for various microwave heating processes.

In addition, waveguides are commonly used as heating apparatuses, which can cause the apparatus to become too large and can impede direct observation of the heating process because it is covered by a metallic body. To solve these problems, previous studies have proposed microwave heating via electromagnetic coupling that does not use a waveguide [22], [23]. This approach to microwave heating is inspired by the electromagnetic field coupling [24], [25] developed for wireless power transfer (WPT) [26]. Electromagnetic resonators with the same resonant frequency become coupled when they are placed in proximity to each other, and this allows the transfer of electromagnetic energy between them. In this method, a portion of the energy transferred between the resonators irradiates the target object, heating it. Because the electromagnetic field between the coupled resonators is used, there is no need to enclose the resonators with metal walls, which allows for the downsizing of the apparatus and the direct observation of the heating process. In addition, the modes generated between the resonators can be calculated in advance, making it possible to use the system for various microwave heating processes. In a previous study [22], two half-wavelength resonators fabricated on dielectric substrates have been used for this type of design. However, the use of a half-wavelength resonator provides uniform heating only in a narrow area.

To extend the range of uniform heating without changing the operation frequency, we previously proposed unifrom microwave heating via electromagnetic coupling using zeroth-order resonators (ZORs) with an infinite guide wavelength [27]. In our previous study, the feasibility of microwave heating via electromagnetically coupled ZORs was investigated only through simulation, and experimental demonstration had not yet been conducted. Furthermore, the matching between the ZORs and the characteristic impedance of 50 Ω was insufficient.

In this paper, we propose an improvement on our previous ZOR design by the addition of a matching circuit to the ZOR. We then report experimental results on the microwave heating of two types of ceramic sheets, composed of SiC and Al_2O_3, using our proposed electromagnetically coupled ZORs to demonstrate its effectiveness. Two typical ceramics are selected and compared from the viewpoint of electrical properties, as the dielectric constant and dielectric loss tangent of SiC are much higher than Al_2O_3.

2. Principles and Design of Zeroth-Order Resonator

The ZOR is composed of a composite right/left-handed transmission line (CRLH-TL) [28]. Figure 1 shows a schematic of the resonant modes when a resonator with an ideal CRLH-TL is excited with both ends open. A feature of this resonator is that it can generate modes with wavenumbers below 0, which is not possible in resonators using solely right-handed lines. Zeroth-order resonance is a resonant mode with a wavenumber of 0. The amplitude and phase in the resonator are uniform, and the guide wavelength in the resonator is infinite. Therefore, neither nodes nor antinodes are generated in the standing wave, enabling uniform heating.

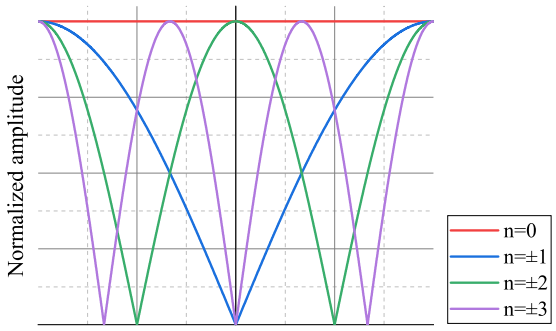

Fig. 1 Resonant modes in a resonator with CRLH-TL

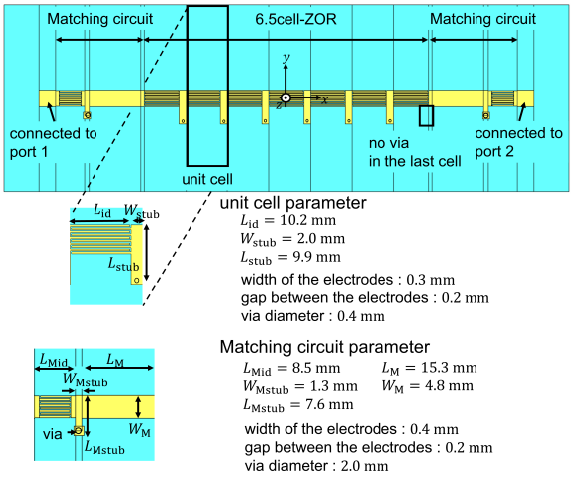

Fig. 2 Layout of the designed 6.5-cell MZOR

Figure 2 shows the designed ZOR. The dielectric substrate of the ZOR was Nippon Pillar NPC-H220A with a thickness of 1.57 mm, a relative permittivity of 2.17, and a loss tangent of 0.0005. In a previous study [29], a 7-cell ZOR with seven cascaded unit cells mounted on a dielectric substrate was considered. In our previous study [27], the short circuit stub in the final cell of the 7-cell ZOR was deleted to achieve a more uniform field distribution by improving the symmetry of the resonator. In both of these studies, the ZOR was coupled to the feed line, which has a characteristic impedance of 50 Ω and a gap of 0.2 mm at both ends to produce shunt-mode resonance by applying open boundary conditions. However, within a few centimeters of the ZOR, the electric field applied at the gaps is large, resulting in a less uniform electric field. Therefore, the equivalent open condition without a gap is considered. In a previous study [30], an interdigital capacitor and an appropriate phase line were used to create equivalent short-circuit conditions for series-mode resonance. In the present study, a matching circuit consisting of interdigital capacitors and stubs was added at both ends of the ZOR to match the characteristic impedance of a 50 Ω system. The feeding was changed from coplanar microstrip feeding to coaxial feeding from the backside of

the substrate. This change was made to eliminate the interference of connectors when reducing the resonator distance and to prevent unwanted coupling at the feeding line sections. Hereafter, the layout with this matching circuit is referred to as a 6.5-cell MZOR.

2.1 Simulations

Simulations of the designed 6.5-cell MZOR shown in Fig. 2 were conducted with CST Studio Suite. The frequency band for the simulations was from 2.4 GHz to 2.5 GHz. The coordinate axes are shown in Fig. 2. The origin was set at the center of the 6.5-cell ZOR on the surface of the substrate. By examining the frequency at which the imaginary part of the Z_{11} component of the impedance matrix becomes zero, we found the zeroth-order resonant frequency of the 6.5-cell MZOR to be 2.48 GHz.

Figure 3 shows the phase of the z-component of the electric field on the plane 5.0 mm from the ZOR in the z-direction. The difference between the maximum and minimum phase values on the ZOR was 38.8°, which is small enough to confirm that the designed ZOR was at or near the zeroth-order resonant state. For comparison, when λ_e represents the effective wavelength of a normal microstrip line of the same width, the resonator length is $0.95\lambda_e$, and the phase difference at both ends of the resonator is 342°.

The electric field amplitude distributions were examined on planes 5.0 mm and 20 mm away from the ZOR in the z-direction. Figure 4 shows the amplitude distributions of electric field in the x-direction at $y = 0$, normalized by their respective maximum values. The ratio between the minimum and maximum were 72.9% and 78.5%, at $z = 5.0$ mm and $z = 20$ mm, respectively. In both results, the range $L_{50\%}$ in which the normalized electric field exceeded $1/\sqrt{2}$ covered the entire 6.5-cell MZOR ($0.95\lambda_g$). The electric field uniformity on the designed ZOR was superior to that of the conventional standing wave ($L_{50\%} = \lambda_g/4$).

2.2 Experiments

We fabricated two 6.5-cell MZORs and measured S-parameters and electric fields. The fabricated 6.5-cell MZORs are shown in Fig. 5. The dielectric substrate was Nippon Pillar NPC-H220A, as in the simulations. We only evaluated the first ZOR for the measurements of the S-parameters and the electric fields.

The measurement system for the electric field distribution is shown in Fig. 6. The S-parameters were measured using a vector network analyzer (Keysight N9929A). Port 1 was connected to the microwave generator (TOKYO KEIKI TZ32ZZDD), and Port 2 was connected to a dummy load. An optical electric field sensor (SEIKO GIKEN ES-130) and its controller (SEIKO GIKEN C5-D1-A) were used to measure the electric field. The measured electric field was monitored

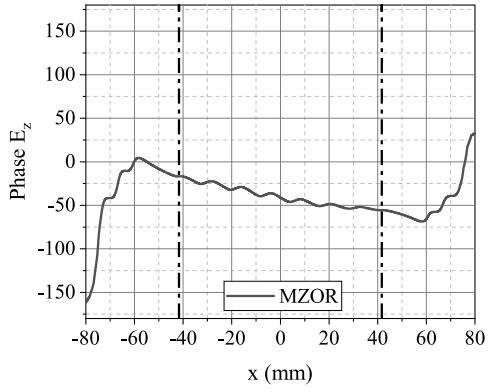

Fig. 3 Phase of the $z-$component of the electric field ($z = 5.0$ mm)

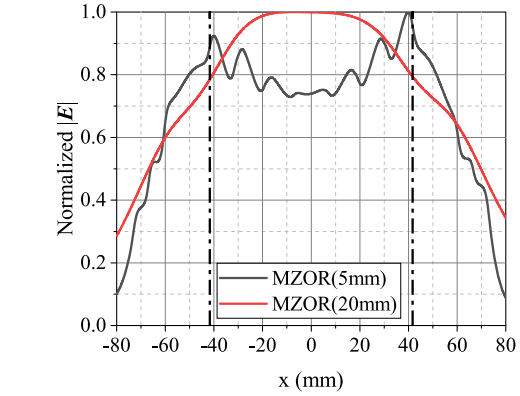

Fig. 4 Distributions of normalized electric field amplitude $|\boldsymbol{E}|$ ($z = 5.0$ mm, 20 mm)

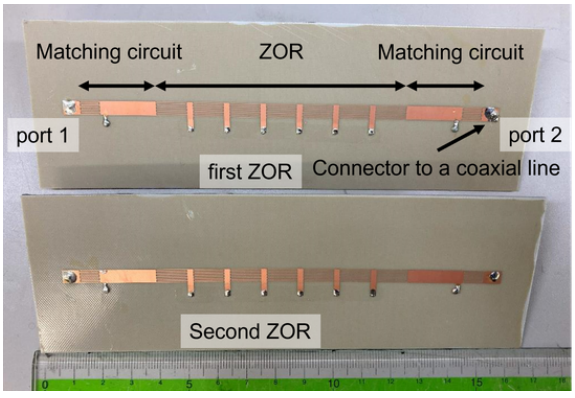

Fig. 5 Photograph of the fabricated 6.5-cell MZORs

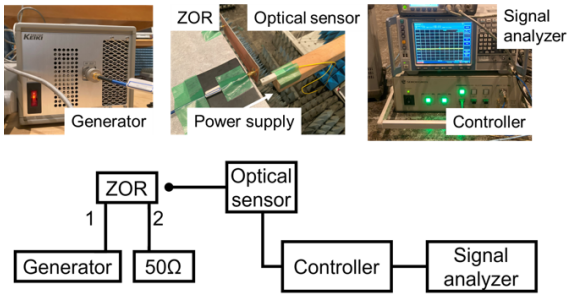

Fig. 6 Electric field measurement system

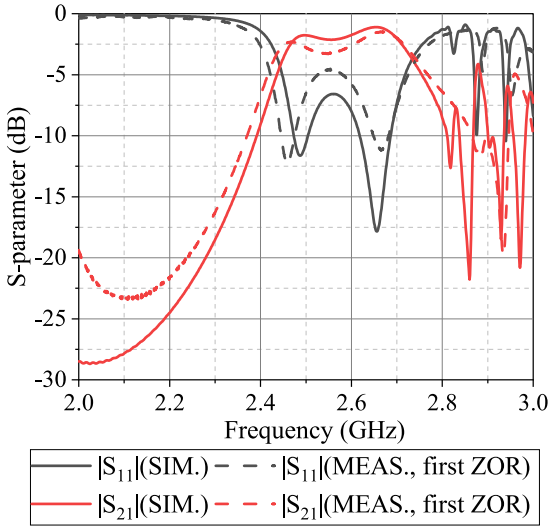

Fig. 7 Measured and simulated S-parameters

by a signal analyzer (ROHDE & SCHWARZ FSV40). The position of the optical electric field sensor was controlled by an antenna tower (DEVICE D2532AV1/O-S). The measurement steps were 2 mm and 5 mm in the x- and y-directions, respectively.

Figure 7 shows the simulation and measurement results of the S-parameters. The results were in good agreement: the zeroth-order resonant frequency was 2.48 GHz in the simulation and 2.45 GHz in the measurement, with an error of 1.22%. By evaluating the simulated electromagnetic field distribution, we determined that the resonance near 2.65 GHz was first-order resonance.

Figure 8 shows the z-component of the normalized electric field in the xy plane 20 mm from the ZOR in the z-direction. The simulation and measurement results are obtained at 2.48 GHz and 2.45 GHz, respectively. The white frames in Fig. 8 (a) indicates the transmission line area of the ZOR. Both the measurement and simulation results reveal an area of high field intensity on the short-circuit stub side ($y < 0$). Around $y = 15$ mm, the z-component of the field intensity is extremely small. This is because the main component of the electric field in this area is in the y-direction.

Figure 8 (b) shows the z-component of the simulated and measured electric fields along the x-axis at three positions along the y-axis. The measurement results are less uniform than the simulation results. The ranges where the normalized z-component of the electric field exceeded $1/\sqrt{2}$ were calculated at each of the three considered y-positions. In the simulation, almost the full range of the ZOR satisfied this condition at the three positions. The measured ranges were 62 mm, 67 mm, and 63 mm at $y = -5$ mm, $y = 0$ mm, and $y = 5$ mm, respectively. Even in the worst case, the experimental results confirm the effectiveness of using the ZOR: the shortest length of 62 mm is equal to $0.51\lambda_0$ at the resonant frequency and is much longer than that of the conventional standing wave ($\lambda_0/4 = 31$ mm), where λ_0 is the free-space wavelength.

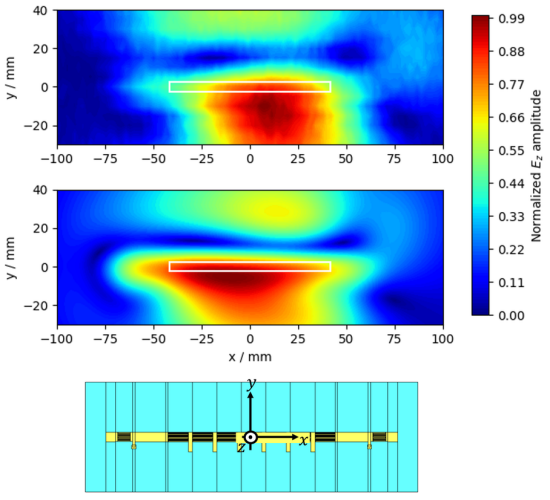

(a) Overall pattern (upper: measured, lower: simulated)

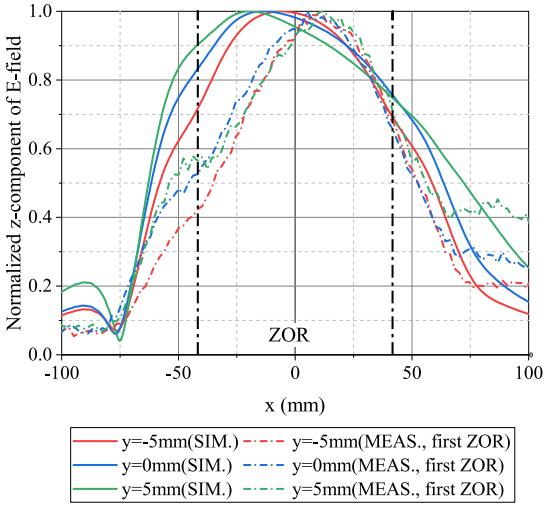

(b) One-dimensional electric field patterns along the x-axis at three positions along the y-axis

Fig. 8 Distribution of the normalized z-component of the electric field at $z = 20$ mm plane (SIM.: 2.48 GHz, MEAS.: 2.45 GHz)

3. Evaluation of Electromagnetic Field Distributions between Electromagnetically Coupled ZORs

The electromagnetic distribution between the electromagnetically coupled ZORs was then evaluated. In the electromagnetic coupling microwave heating system, two resonators are placed facing each other for electromagnetic coupling, and a sample placed between the resonators is heated. In this initial evaluation, two ZORs were placed facing each other for electromagnetic coupling, but the heated object was omitted for the sake of understanding the electromagnetic coupling of the ZORs in the unloaded condition.

Figure 9 shows the proposed heating apparatus. The structure of the two evaluated 6.5-cell MZORs is symmetrical about the $z = 0$ plane. The input port was set at one terminal of the first ZOR, and its other terminal was shorted

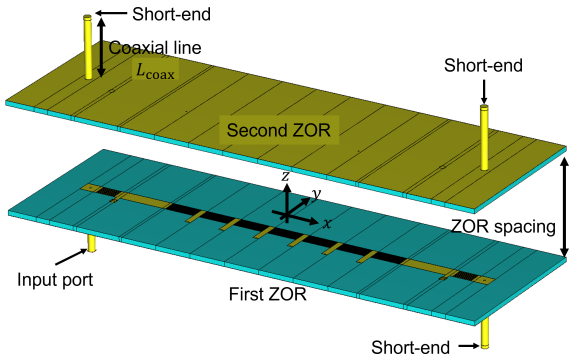

Fig. 9 Proposed heating apparatus

through a coaxial line. In the second ZOR, both terminals were shorted through a coaxial line. These short-end coaxial lines contribute to enhancing the microwave heating efficiency by reusing the reflection of microwaves. Because the electromagnetic field distribution between ZORs varies with the ZOR spacing and the coaxial line length L_{coax}, these parameters were varied to obtain optimal values.

The evaluation index U was used to calculate the optimal value and is given by

$$U = \int_L \left| \frac{\partial |\boldsymbol{E}|}{\partial x} \right| \mathrm{d}x \Big/ \frac{1}{L} \int_L |\boldsymbol{E}| \mathrm{d}x, \tag{1}$$

where L is the integral range and $\boldsymbol{E}$ is the electric field. The evaluation index was defined with two objectives: the uniformity of the electric field distribution and the heating efficiency. In this way, it evaluates the effectiveness of the electromagnetic field distribution in realizing uniform heating. From the viewpoint of the uniformity of the electric field distribution, the fluctuation of the electric field intensity should be small and constant within the heating range. From the viewpoint of heating efficiency, the electric field intensity should be high. As the uniformity increases, the numerator of U decreases, whereas as the field intensity increases, the denominator increases. Therefore, U should be small for uniform heating.

The length of the ZOR in the x-direction is 85.4 mm, and the integral range was set to $-38.43\,\mathrm{mm} < x < 38.43\,\mathrm{mm}$, which corresponds to 90% of the resonator length. Arranging two identical ZORs to face each other reduced the resonant frequency from 2.48 GHz in the single two-port model to 2.45 GHz. Therefore, the electromagnetic field distribution in this section was evaluated at 2.45 GHz.

3.1 Coaxial Line Length

Under a fixed ZOR spacing of 25 mm, the coaxial line length L_{coax} was swept. The impedance from the substrate surface to the short end of the coaxial line varied with L_{coax}, indicating that the phase of the reflected wave changes and affects the resonant mode. We investigated this relationship in the range $0 < L_{coax} < \lambda_g/2$, where λ_g is the guide wavelength in the coaxial line, because the imaginary part of the impedance varies from $-\infty$ to ∞ in this range.

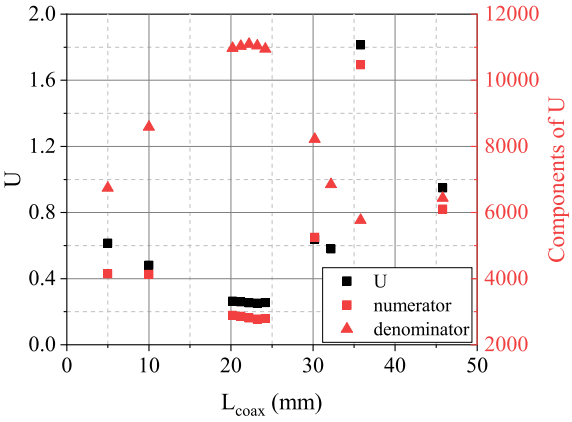

Fig. 10 U and its components plotted against L_{coax}

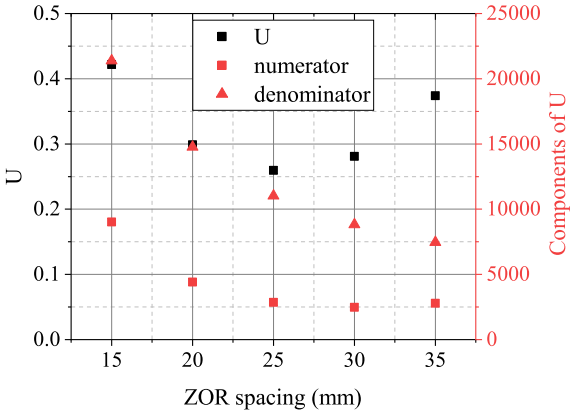

Fig. 11 U and its components plotted against ZOR spacing

Figure 10 shows the evaluation index U and its numerator and denominator plotted against L_{coax}. U was small when L_{coax} was approximately 22 mm ± 2 mm. In this range, both the numerator and the denominator were confirmed to take on optimal values. Because the guide wavelength of the coaxial line at 2.45 GHz is 84.4 mm, L_{coax} should be approximately $\lambda_g/4$ at the resonant frequency. This result is explained by the interference between the incident and reflected waves. When L_{coax} is $\lambda_g/4$, the incident wave returns to the entrance of the coaxial line with a phase shift of 2π because of the round trip of the coaxial line and the reflection at the short-circuit end. The resultant wave generated without cancellation maintains the original waveform, resulting in a resonance state that is uniform and has a large electric field intensity.

3.2 ZOR Spacing

Under a fixed L_{coax} of $\lambda_g/4$, the ZOR spacing was swept at 5 mm intervals. Figure 11 shows the evaluation index U and its numerator and denominator plotted against the ZOR spacing. The numerator of U tended to decrease as the ZOR spacing was increased when the ZOR spacing was less than 25 mm. However, when the ZOR spacing was

increased beyond 25 mm, the numerator remained approximately constant. The denominator monotonically decreased with increasing ZOR spacing. From the above results, a ZOR spacing of 25 mm was selected to minimize the evaluation index U.

4. Simulations Including Heated Objects

Simulations including heated objects were performed under the optimal resonator spacing of 25 mm and coaxial line length of 21.1 mm. Figure 12 shows the simulation model. The heated object was placed in the center between the resonators, which was defined as the $z = 0$ plane, and aligned with the ZORs and the central axis.

Sheets of SiC and Al_2O_3 were considered as the heated objects. The values of the relative permittivity ε_r and loss tangent $\tan\delta$ at 2.5 GHz used in the simulations of these materials are listed in Table 1 [31]. The dimensions of the heated objects were set to 50 mm in the x- and y-directions and 1 mm in the z-direction.

To evaluate the performance of the heating apparatus, the three power ratios P_A, P_L, and P_O were calculated according to the destination of the power consumption, where P_A, P_L, and P_O represent the proportions of the power absorbed by the heated object, leaked from the apparatus, and consumed by the apparatus, respectively. These power ratios were calculated as a percentage of the power received by the apparatus, excluding the reflected power. To evaluate the heating uniformity, the evaluation index $L_{50\%}$ was calculated as the range within which the power loss density in the sheet was greater than 50% of the maximum value. The power loss density was calculated along the x-axis at $y = z = 0$.

The simulation results of the power ratios are given in Table 2. The power ratios for the SiC and Al_2O_3 objects differed significantly from each other. The energy loss in the dielectric P_D is given by

$$P_D = 2\pi f \varepsilon_0 \varepsilon_r |\boldsymbol{E}|^2, \tag{2}$$

where f is the operation frequency, ε_0 is the permittivity of free space, and $\boldsymbol{E}$ is the electric field. From (2), dielectrics with large ε_r and $\tan\delta$ are easily heated. A comparison of the power ratios for SiC and Al_2O_3 reveals that whereas SiC absorbs approximately $P_A = 16\%$, this is reduced to near zero for Al_2O_3, and this reduction in power absorption is equally distributed to P_L and P_O (Table 2). Therefore, the Al_2O_3 object is heated with substantially lower efficiency, and the apparatus itself generates heat. The breakdown of P_O was calculated to be approximately 20% and 78% for the dielectric substrate and copper foil, respectively, and approximately 2% for the dielectric (PTFE) in the coaxial line for both heating materials.

Next, we considered P_L, which accounts for more than 60% of the total power for both heated objects. As shown in Fig. 12, four planes were set up to surround the heating apparatus, and the power leakage was examined by integrating the normal component of the Poynting vector for each plane. Table 3 gives the percentage for each plane. The leakage was large in the $\pm Y$ plane along the longitudinal direction of the ZOR, and the ratio was especially high in the $-Y$ plane, which is the short-circuit stub side. This is explained by the fact that the ZOR resonates in shunt mode and current flows through the short-circuit stub, so that the stub behaves as a radiation source.

Figure 13 shows the normalized power loss density distribution at the center of the heated object. For both heated objects, nonuniform heating due to nodes and antinodes in standing waves was never observed, and a power loss density of more than 50% of the maximum value could be achieved over a wide range. In the case of dielectric heating using a waveguide, $L_{50\%}$ is equal to $\lambda_g/4$. For each of the considered materials, the value of $L_{50\%}$ obtained from the simulation re-

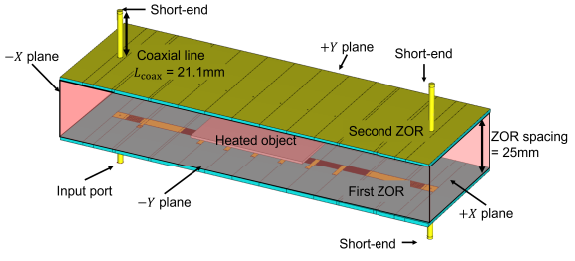

Fig. 12 Simulation model including a heated object with the definition of the $\pm X$ and $\pm Y$ planes

Table 1 Values of ε_r and $\tan\delta$ used in simulations

	ε_r	$\tan\delta$
SiC	60	0.58
Al_2O_3	9.9	0.0001

Table 2 Simulation results with SiC and Al_2O_3 heated objects

	P_A	P_L	P_O	$L_{50\%}$
SiC	16.6%	62.1%	21.3%	48.6 mm
Al_2O_3	0.00103%	70.6%	29.4%	50 mm

Table 3 Proportion of P_L in various planes

	$-Y$ plane	$+Y$ plane	$-X$ plane	$+X$ plane
SiC	66.5%	28.3%	2.19%	3.00%
Al_2O_3	67.2%	27.7%	2.18%	2.86%

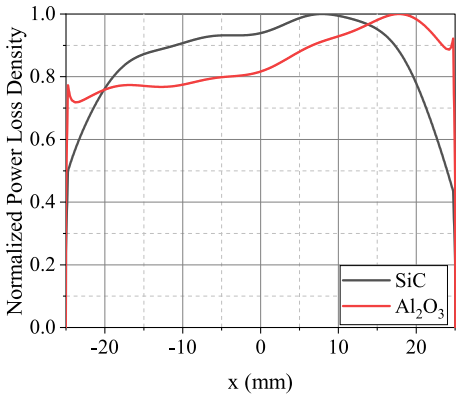

Fig. 13 Normalized power loss density distribution

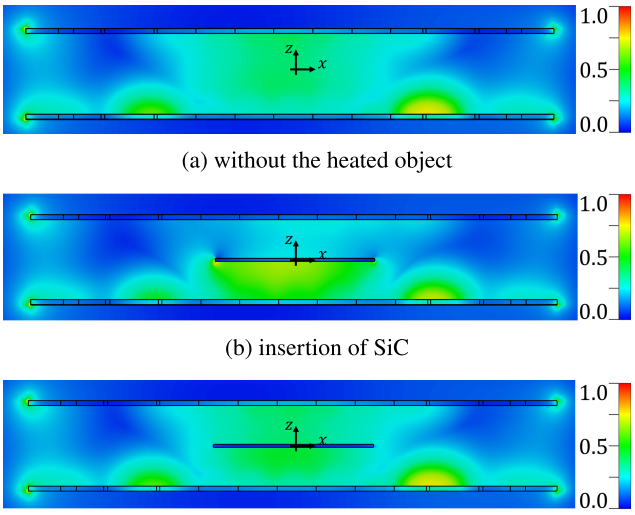

(a) without the heated object

(b) insertion of SiC

(c) insertion of Al_2O_3

Fig. 14 Normalized electric field amplitude distribution at the plane $y = -12.5$ mm

sults was $0.397\lambda_0$ for SiC and $0.409\lambda_0$ for Al_2O_3, and $L_{50\%} > \lambda_0/4$ for both heated objects. This result demonstrates that the use of ZOR is effective in terms of uniform heating.

Variations of the electric field distribution between the resonators with the insertion of the heated object are evaluated. Figure 14 shows the simulation results of electric field amplitude distributions at $y = -12.5$ mm. While there was only a slight change in the case of Al_2O_3, there was a difference in the electric field amplitude distributions in the case of SiC. When SiC was inserted, the electric field amplitude between the heated object and the second resonator became smaller. This is because the large absorption of microwave power in SiC weakens the coupling between the resonators. In addition, the asymmetry properties of the power loss density distribution shown in Fig. 13 is caused by the asymmetry properties of the electric field in the $x-$direction in the heated object shown in Fig. 14. This asymmetry would be attributed to the difference of the boundary conditions between the tangential and normal components of the electric field. The $z-$component of the electric field, which is the main component of uniform electric field, is the normal component to the heated objects. Hence, the electric field of the normal component inside the objects would decrease on the boundary between the object and air, and the electric field of the tangential components would relatively affect the power loss density.

5. Heating Experiments

Heating experiments were conducted to validate the simulation results. The heated objects were 50 mm square sheets of SiC and Al_2O_3, as in the simulation. Bamboo tongs were used to fix the position of the heated objects. The experimental system is shown in Fig. 15. With a fiber-optic thermometer (ANRITSU FL-2400), four points were measured: the GND surface of the first ZOR, in which the input port was set, the GND surface of the other ZOR, and the first

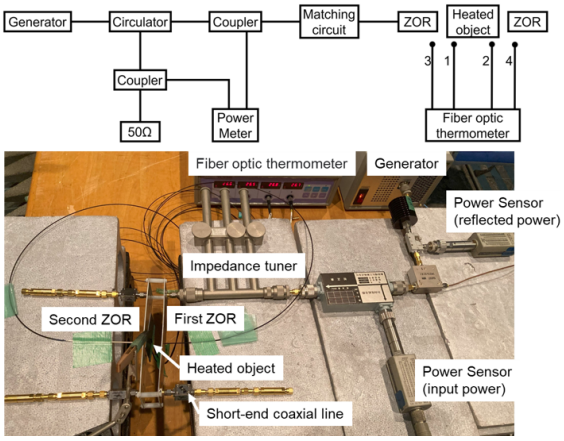

Fig. 15 Measurement setup for heating experiments

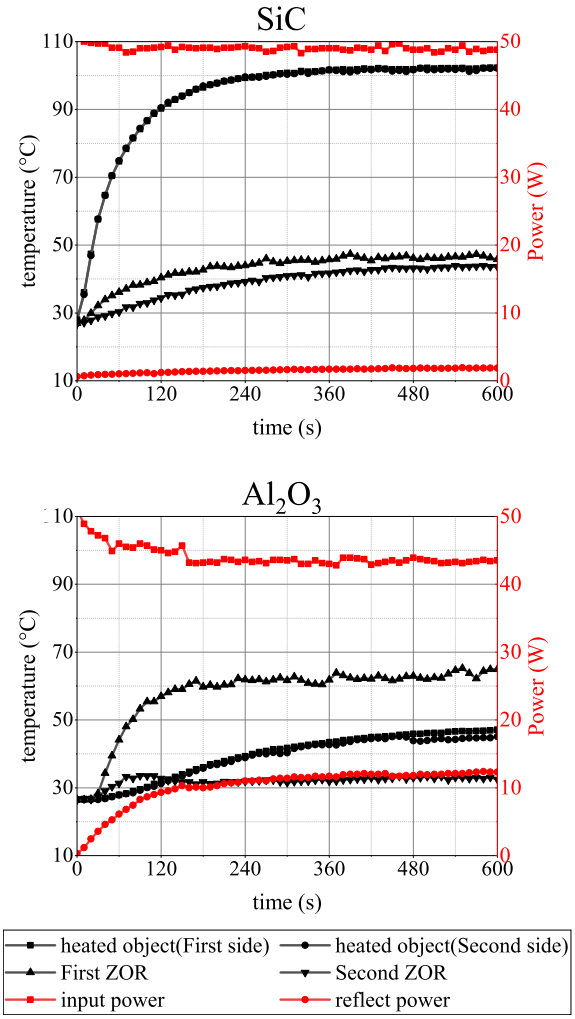

Fig. 16 Measured temperature and power (upper: SiC, lower: Al_2O_3)

and second sides of the heated object. Fiber-optic probes were used to measure the heated object (ANRITSU FS100-M), the first ZOR (ANRITSU FSC150-2M), and the second ZOR (FS400-3M). The input and reflected power were mea-

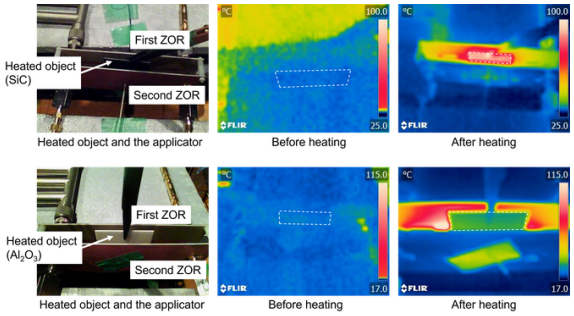

Fig. 17 Temperature distribution before the heating and after the 600-seconds heating (upper: SiC, lower: Al_2O_3)

sured using power sensors (Agilent N8481H) connected to a power meter (Agilent 1914A). Variable-length coaxial lines were attached to the three ports other than the input port. Based on the results in Sect. 3.1, $L_{\mathrm{coax}} = \lambda_{\mathrm{g}}/4$ is appropriate, so the impedance estimated from the connection to the end was adjusted to be infinite.

Figure 16 shows the measurement results for 10 minutes of heating at an input power of 50 W at 2.45 GHz. As in the simulation results, the temperature of the SiC heated object increased, whereas in the case of the Al_2O_3 object, the first ZOR showed the greatest temperature increase, and the temperature of the heated object did not increase at all. The reflected power did not change significantly with the SiC object but showed larger changes with the Al_2O_3 object, possibly due to the temperature rise of the first ZOR and the change in input impedance caused by the temperature difference between the two resonators.

Figure 17 shows the temperature distribution before the heating and after the 600-seconds heating, as observed by an infrared camera (FLIR C2EKJ). The white dotted frames in Fig. 17 indicates the area of heating objects. Both heated objects have a uniform temperature distribution. The temperature rise of the SiC heated object is apparent in this figure, whereas the temperature of the Al_2O_3 heated object did not change so much, and the change in the first ZOR was large. These results are the same as other results obtained by simulation and thermometer measurements.

6. Conclusion

In this study, we proposed microwave heating via electromagnetic coupling using zeroth-order resonators (ZORs) as a microwave heating device capable of uniformly heating a wide area. First, the characteristics of the zeroth-order resonant state generated in a 6.5-cell ZOR including a matching circuit (6.5-cell MZOR) were investigated by simulation. After determining the optimal resonator spacing and coaxial line length under the electromagnetic coupling from the simulation results, heating simulations of the ceramic substrate were performed. The 6.5-cell MZORs were fabricated, and the generation of zeroth-order resonance was confirmed from the input–output characteristics and measured electric field distribution. To investigate the feasibility of the simulation results, heating experiments were performed on objects composed of SiC and Al_2O_3 at 50 W for 10 minutes. A temperature rise of more than 75 °C was confirmed for the SiC object, which was easily heated, but only 18 °C was observed for the Al_2O_3 object, reflecting the simulation results.

Extension of the ZOR length will be a future work for practical applications. From electromagnetic simulations, the evaluation indices U in (1) were 0.259, 0.263 and 2.40 in the cases of 6.5-cell ZOR fabricated in this study, 10-cell ZOR and 15-cell ZOR, respectively. Therefore, the 10-cell ZOR, the ZOR length of 120 mm, is available as the proposed heating system, but the 15-cell ZOR, the ZOR length of 180 mm, is difficult to use in the current system. Other types of ZORs including waveguides will be candidates for practical use.

Acknowledgments

This work was supported by JSPS KAKENHI Grant Number JP21K04175. Experimental measurements were conducted through the collaborative research facilities: the Analysis and Development System for Advanced Materials (ADAM) and the Microwave Energy Transmission Laboratory (METLAB), in the Research Institute for Sustainable Humanosphere (RISH), Kyoto University.

References

[1] S. Chandrasekaran, S. Ramanathan, and T. Basak, "Microwave food processing—A review," Food research international, vol.52, no.1, pp.243–261, 2013.
[2] S.A. Galema, "Microwave chemistry," Chemical Society Reviews, vol.26, no.3, pp.233–238, 1997.
[3] M. Miura, H. Kaga, A. Sakurai, T. Kakuchi, and K. Takahashi, "Rapid pyrolysis of wood block by microwave heating," Journal of Analytical and Applied Pyrolysis, vol.71, no.1, pp.187–199, 2004.
[4] W. Puacz, W. Szahun, and M. Kopras, "Application of microwave heating to the determination of free, combined and total sulphur in rubber," Talanta, vol.42, no.12, pp.1999–2006, 1995.
[5] S. Das, A.K. Mukhopadhyay, S. Datta, and D. Basu, "Prospects of microwave processing: An overview," Bulletin of materials science, vol.32, pp.1–13, 2009.
[6] D.K. Agrawal, "Microwave processing of ceramics," Current Opinion in Solid State and Materials Science, vol.3, no.5, pp.480–485, 1998.
[7] M. Oghbaei and O. Mirzaee, "Microwave versus conventional sintering: A review of fundamentals, advantages and applications," Journal of alloys and compounds, vol.494, no.1-2, pp.175–189, 2010.
[8] J.D. Katz, "Microwave sintering of ceramics," Annual Review of Materials Science, vol.22, no.1, pp.153–170, 1992.
[9] M.S. Spotz, D.J. Skamser, and D.L. Johnson, "Thermal Stability of Ceramic Materials in Microwave Heating," Journal of the American Ceramic Society, vol.78, no.4, pp.1041–1048, 1995.
[10] E. Thostenson and T.-W. Chou, "Microwave processing: fundamentals and applications," Composites Part A: Applied Science and Manufacturing, vol.30, no.9, pp.1055–1071, 1999.
[11] P. Plaza-Gonzalez, J. Monzo-Cabrera, J.M. Catala-Civera, and D. Sanchez-Hernandez, "Effect of Mode-Stirrer Configurations on Dielectric Heating Performance in Multimode Microwave Applicators," IEEE Trans. Microw. Theory Techn., vol.53, no.5, pp.1699–1706, 2005.
[12] P. Plaza-González, J. Monzó-Cabrera, J.M. Catalá-Civera, and D.

Sánchez-Hernández, "New Approach for the Prediction of the Electric Field Distribution in Multimode Microwave-Heating Applicators with Mode Stirrers," IEEE Trans. Magn., vol.40, no.3, pp.1672–1678, 2004.
[13] S.S.R. Geedipalli, V. Rakesh, and A.K. Datta, "Modeling the heating uniformity contributed by a rotating turntable in microwave ovens," Journal of food engineering, vol.82, no.3, pp.359–368, 2007.
[14] S.-H. Bae, M.-G. Jeong, J.-H. Kim, and W.-S. Lee, "A Continuous Power-Controlled Microwave Belt Drier Improving Heating Uniformity," IEEE Microw. Compon. Lett., vol.27, no.5, pp.527–529, 2017.
[15] S.-H. Ahn, C.-H. Jeong, D.-M. Lim, and W.-S. Lee, "Kilowatt-Level Power-Controlled Microwave Applicator with Multiple Slotted Waveguides for Improving Heating Uniformity," IEEE Trans. Microw. Theory Techn., vol.68, no.7, pp.2867–2875, 2020.
[16] J. He, Y. Yang, H. Zhu, K. Li, W. Yao, and K. Huang, "Microwave heating based on two rotary waveguides to improve efficiency and uniformity by gradient descent method," Applied Thermal Engineering, vol.178, p.115594, 2020.
[17] P.E. Parris and V.M. Kenkre, "Thermal Runaway in Ceramics Arising from the Temperature Dependence of the Thermal Conductivity," physica status solidi (b), vol.200, no.1, pp.39–47, 1997.
[18] H. Kato, Y. Kobayashi, W. Iijima, K. Takekura, K. Shigeta, and K. Yakushido, "Study of Microwave Pretreatment on Oil Expression Facilities Investigation on Continuous Heating of Rapeseed using the Rectangular Waveguide Microwave Applicator (in Japanese)," Nogyo Shisetsu (Journal of the Society of Agricultural Structures, Japan), vol.44, no.1, pp.1–6, 2013.
[19] K.A. Lurie and V.V. Yakovlev, "Method of control and optimization of microwave heating in waveguide systems," IEEE Trans. Magn., vol.35, no.3, pp.1777–1780, 1999.
[20] R. Heeren and J. Baird, "An Inhomogeneously Filled Rectangular Waveguide Capable of Supporting TEM Propagation (Correspondence)," IEEE Trans. Microw. Theory Techn., vol.19, no.11, pp.884–885, 1971.
[21] S. Jung, J.H. Kwak, and S.M. Han, "Guided-wavelength-controlled dynamic microwave heating in a near-cutoff waveguide," Applied Thermal Engineering, vol.188, p.116630, 2021.
[22] T. Mitani, D. Nishio, and N. Shinohara, "Feasibility Study on a Microwave Heating Applicator Using Electromagnetic Coupling," 2018 Asia-Pacific Microwave Conference, pp.1142–1144, 2018.
[23] T. Toyonaga, T. Mitani, and N. Shinohara, "Study on Electromagnetic Coupling-Type Microwave Heating Systems with Repeaters," 2022 Asia-Pacific Microwave Conference, pp.662–664, 2022.
[24] J.-S. Hong, "Couplings of asynchronously tuned coupled microwave resonators," IEE Proceedings: Microwaves, Antennas and Propagation, vol.147, no.5, pp.354–358, 2000.
[25] N. Shinohara, "The wireless power transmission: inductive coupling, radio wave, and resonance coupling," Wiley Interdisciplinary Reviews: Energy and Environment, vol.1, no.3, pp.337–346, 2012.
[26] N. Shinohara, "Power without wires," IEEE Microw. Mag., vol.12, no.7, pp.S64–S73, 2011.
[27] B. Takahara, T. Mitani, and N. Shinohara, "Feasibility Study on Electromagnetic Coupled Type Uniform Microwave Heating Using a Zeroth-Order Resonator," 2022 Asia-Pacific Microwave Conference, pp.665–667, 2022.
[28] A. Lai, T. Itoh, and C. Caloz, "Composite right/left-handed transmission line metamaterials," IEEE Microw. Mag., vol.5, no.3, pp.34–50, 2004.
[29] A. Sanada, C. Caloz, and T. Itoh, "Novel zeroth-order resonance in composite right/left-handed transmission line resonators," 2003 Asia-Pacific Microwave Conference, pp.1588–1591, 2003.
[30] A. Rennings, T. Liebig, S. Otto, C. Caloz, and I. Wolff, "Highly Directive Resonator Antennas Based on Composite Right/Left-handed (crlh) Transmission Lines," 2007 2nd International ITG Conference on Antennas, pp.190–194, 2007.
[31] Y. Takeuchi, T. Abe, T. Kageyama, and H. Sakai, "Rf dielectric properties of sic ceramics and their application to design of hom absorbers," Proceedings of the 2005 Particle Accelerator Conference, pp.1195–1197, 2005.

Baku Takahara received the B.E. degree in electrical and electronic engineering from Kyoto University, Japan, in 2022. He is currently pursuing the M.E. degree in electrical engineering. His current reserch interests include uniform microwave heating using metamaterial.

Tomohiko Mitani received the B.E. degree in electrical and electronic engineering, the M.E. degree in informatics, and the Ph.D. in electrical engineering from Kyoto University, Kyoto, Japan, in 1999, 2001, and 2006, respectively. He was an Assistant Professor with the Radio Science Center for Space and Atmosphere, Kyoto University, in 2003. He has been an Associate Professor with the Research Institute for Sustainable Humanosphere, Kyoto University, since 2012. His current research interests include microwave heating application and microwave power transfer. He was a board member of Japan Society of Electromagnetic Wave Energy Applications (JEMEA) from 2014 to 2024. He was a treasurer of IEEE MTT-S Kansai Chapter from 2014 to 2017, and from 2019 to 2021. He has been a technical committee chair of IEEE MTT-S Kansai Chapter since 2022.

Naoki Shinohara received the B.E. degree in electronic engineering, the M.E. and Ph.D (Eng.) degrees in electrical engineering from Kyoto University, Japan, in 1991, 1993 and 1996, respectively. He was a research associate in Kyoto University from 1996. From 2010, he has been a professor in Kyoto University. He has been engaged in research on Solar Power Station/Satellite and Microwave Power Transmission system. He was IEEE MTT-S Distinguish Microwave Lecturer (2016–18), and is IEEE AdCom member (2022–2024), IEEE MTT-S Technical Committee 25 (Wireless Power Transfer and Conversion) former chair and member, IEEE MTT-S MGA (Member Geographic Activities) Region 10 regional coordinator, IEEE WPT Initiative Member, IEEE MTT-S Kansai Chapter TPC member, IEEE Wireless Power Transfer Conference founder and Steering committee member, URSI commission D past chair, international journal of Wireless Power Transfer (Hindawi) executive editor, the first chair and technical committee member on IEICE Wireless Power Transfer, Japan Society of Electromagnetic Wave Energy Applications former president and adviser, Space Solar Power Systems Society president, Wireless Power Transfer Consortium for Practical Applications (WiPoT) chair, and Wireless Power Management Consortium (WPMc) chair. His books are "Wireless Power Transfer via Radiowaves" (ISTE Ltd. and John Wiley & Sons, Inc.), "Recent Wireless Power Transfer Technologies Via Radio Waves (ed.)" (River Publishers), and "Wireless Power Transfer: Theory, Technology, and Applications (ed.)" (IET), and some Japanese text books of WPT.